Journal of the European Ceramic Society 45 (2025) 116936

Contents lists available at ScienceDirect

Journal of the European Ceramic Society

journal homepage: www.elsevier.com/locate/jeurceramsoc

Ga-ion migration during co-sintering of heterogeneous Ta- and Ga-substituted LLZO solid-state electrolytes

Walter Sebastian Scheld [a,*], Yannic Collette [a,b], Christian Schwab [a], Martin Ihrig [a], Sven Uhlenbruck [a,c], Martin Finsterbusch [a,c], Dina Fattakhova-Rohlfing [a,b,c,**]

[a] Forschungszentrum Jülich GmbH, Institute of Energy Materials and Devices, Materials Synthesis and Processing IMD-2, Jülich 52425, Germany
[b] University of Duisburg-Essen, Faculty of Engineering and Center for Nanointegration Duisburg-Essen CENIDE, Lotharstraße 1, Duisburg 47057, Germany
[c] Jülich Aachen Research Alliance JARA-ENERGY, Jülich 52425, Germany

ARTICLE INFO

Keywords:
Solid-state electrolyte
Ceramic
$Li_7La_3Zr_2O_{12}$
Garnet
Co-sintering
Heterogeneous electrolyte

ABSTRACT

$Li_7La_3Zr_2O_{12}$ (LLZO) is an attractive solid-state electrolyte for next-generation lithium solid-state batteries (SSB) because of its high ionic conductivity, and safety properties. Only the cubic LLZO phase has sufficient ionic conductivity, which is stabilized by substitution with elements like Ta or Ga. Ga-substituted LLZO has the highest ionic conductivity but is not stable towards metallic Li anodes, while Ta-substituted LLZO has a slightly lower conductivity but excellent reduction stability towards Li anodes. The combination of LLZO:Ga as a catholyte and LLZO:Ta as a ceramic separator for Li anodes would significantly enhance the performance of SSBs, but both materials have different processing parameters. In this work, the possibility of co-sintering LLZO:Ga|LLZO:Ta components is investigated with varying Li-excess of the LLZO:Ta phase, while the results are compared with pure references. The experiments showed a changed sintering activity, secondary phase formation, Ta- and Ga-ion diffusion, and a changed ionic conductivity when co-sintering LLZO:Ga|LLZO:Ta.

1. Introduction

Solid-state Li batteries (SSBs) have great potential to be the next generation of electrochemical energy storage technology in terms of safety and chemical stability [1]. In a transition from liquid to solid electrolytes, unrivaled thermal stability and higher energy densities can be achieved [1–4]. Among the different material classes of solid-state electrolytes, the oxide ceramic materials such as $Li_7La_3Zr_2O_{12}$ (LLZO) attract attention as they exhibit high reduction stability that allows the use of Li metal anodes, and show a high ionic conductivity of about 10^{-3} S cm^{-1} at room temperature [5,6]. As an oxide, the LLZO has a high thermal stability and is non-flammable, enabling high safety at the cell level [5,6]. The high ionic conductivity can only be achieved in the high-temperature cubic phase of LLZO, as the tetragonal phase has low ionic conductivity [7,8]. A general strategy to stabilize the cubic phase is the substitution [9] of Li-, La-, or Zr-sites in the LLZO structure with elements such as Ta [10–12], Y [11], Cr [13], Te [14], Nb [12,15], Al [16,17], Ge [7], Ga [18–20] and others [9]. The choice of substituent has a direct influence on the properties of the electrolyte, but also on the synthesis conditions and processing parameters [7,10–18]. Ga-substitution (LLZO:Ga) leads to one of the highest ionic conductivities and is therefore advantageous for cell applications [21]. However, the solubility of Ga-ion in LLZO is limited and excess Ga precipitates at the LLZO grain boundaries as $LiGaO_2$ [19]. Furthermore, in Li-rich systems the Ga-ions can be expelled in a slow process, leaving tetragonal LLZO with oxygen vacancies residuals and decreased Li-ion conductivity [19]. Therefore, LLZO:Ga is much more sensitive to the excess Li concentration (Li excess) in the powder during sintering [19] compared to e.g. Ta-substituted LLZO (LLZO:Ta) [10–12]. The major drawback of the $LiGaO_2$ is the instability with Li metal, where Li_2Ga and Li_2O are formed, and the resulting volume change causes significant stresses that break up the electrolyte along the grain boundaries [19]. An approach to improve the stability of LLZO:Ga towards Li metal was suggested by Li et al. [19]. The authors used SiO_2 as an additive, which reacts with the Li-ions from the $LiGaO_2$ phase to form the thermodynamically more stable Li_2SiO_3, while the Ga-ions diffuse into the LLZO

* Corresponding author.
** Corresponding author at: Forschungszentrum Jülich GmbH, Institute of Energy Materials and Devices, Materials Synthesis and Processing IMD-2, Jülich 52425, Germany.
E-mail addresses: s.scheld@fz-juelich.de (W.S. Scheld), d.fattakhova-rohlfing@fz-juelich.de (D. Fattakhova-Rohlfing).

https://doi.org/10.1016/j.jeurceramsoc.2024.116936
Received 29 May 2024; Received in revised form 14 August 2024; Accepted 20 September 2024
Available online 20 September 2024
0955-2219/© 2024 The Authors. Published by Elsevier Ltd. This is an open access article under the CC BY license (http://creativecommons.org/licenses/by/4.0/).

structure [19]. However, the incorporation of SiO_2 increases the complexity of the synthesis, and the resulting Li_2SiO_3 increases the mass of the passive components in the final full cell system, thus lowering the energy density. In addition, side reactions of the various cathode materials with silica and the lithium silicate additive are conceivable.

Therefore, other options without additional additives would be more suitable for the application of LLZO:Ga in practical cells. An attractive and widely discussed possibility is to use different LLZO materials for different functions in the cell. For example, LLZO:Ga with its high ionic conductivity could be used as a catholyte in the composite cathode [10, 22–24], while another type of LLZO with high stability towards Li metal, such as LLZO:Ta, could be used as anolyte in the separator [10–12]. A schematic setup of such a cell is shown in Fig. 1a.

The fabrication of ceramic LLZO components is commonly achieved in a sintering step at elevated temperatures with long dwell times [7, 10–18]. Since the sintering parameters and the required Li excess for LLZO:Ga and LLZO:Ta are different [10–12,18,19] its questionable if the presented setup of Fig. 1 is possible to fabricate. Substituents could diffuse during sintering, resulting in a decreased ionic conductivity due to tetragonal LLZO formation, and additionally $LiGaO_2$ could be formed in the LLZO:Ta separator reducing its stability to Li metal. To test the suitability of a heterogeneous electrolyte cell design with LLZO:Ga and LLZO:Ta, powders of both materials were pressed on top of each other and co-sintered as shown in Fig. 1b. The resulting heterogeneous electrolyte pellets were evaluated of their ionic conductivity, chemical phases, ion distribution and microstructure. Additionally, the amount of Li excess in the LLZO:Ta powder was varied.

2. Experimental

2.1. Powder synthesis

Ta-substituted and LLZO with a slight Al addition ($Li_{6.45}Al_{0.05}La_3Zr_{1.6}Ta_{0.4}O_{12}$, referred to hereafter as LLZO:Ta), and Ga-substituted LLZO ($Li_{6.4}Ga_{0.2}La_3Zr_2O_{12}$) powder was prepared by a three-step solid-state reaction [20,25–27]. The base starting materials $LiOH{\bullet}H_2O$ (Applichem, 99.00 %), La_2O_3 (Merck, 99.90 %, predried at 900 °C for 10 h), ZrO_2 (Treibacher, 99.70 %), and the substituent educts Ta_2O_5 (Treibacher, 99.99 %), Al_2O_3 (Inframat, 99.82 %), and Ga_2O_3 (Alfa Aesar, 99.99 %) were dry-milled and stoichiometrically mixed. For the LLZO:Ta powder three batches with varying Li excess was weight: 0 mol % (LLZO:Ta 0 %) and 10 mol% (LLZO:Ta 10 %) $LiOH{\bullet}H_2O$, while the LLZO:Ga was prepared only without Li excess. The powders were individually pressed into pellets (uniaxial, Ø 45 mm, 19 MPa) and calcined in an Al_2O_3 crucible at 850 °C and 1000 °C for 20 h each. In between the calcination steps, the powder was ground and pressed.

For the co-sintering experiments the LLZO:Ga and the different LLZO:Ta powders were stacked in the dye and pressed (uniaxial, Ø 13 mm, 113 MPa) and afterwards sintered in an Al_2O_3 crucible with a MgO plate and a LLZO:Ta (same powder as the bottom layer) powder sheet at 1200 °C with a dwell time of 4 h.

For the manufacturing with field assisted sintering, also known as spark plasma sintering (FAST/SPS) 1 g of LLZO:Ta powder was filled into a mould with an inner diameter of 12 mm made of molybdenum based alloy TZM (Plansee SE) that was covered by wound graphite foil (SGL Carbon). This powder was loosely hand-pressed with fitting punches. Afterwards, around 1 g LLZO:Ga powder was added and adjacently pressed again. The die was then closed with the fitting punches (covered by graphite foil). The pressed powders were sintered in a HP D 5 FAST/SPS device (FCT Systeme). The sintering was performed at a temperature of 675 °C with 10 min dwell time in Ar flow and an applied mechanical pressure of 440 MPa. The heating rate was 100 K min^{-1} and the cooling was 20 K min^{-1}. The FAST/SPS parameter were selected based on our previous work which showed that these parameters are beneficial for sintering of LLZO at low temperature that allows to avoid significant ionic cross-diffusion or loss of volatile elements [24,28].

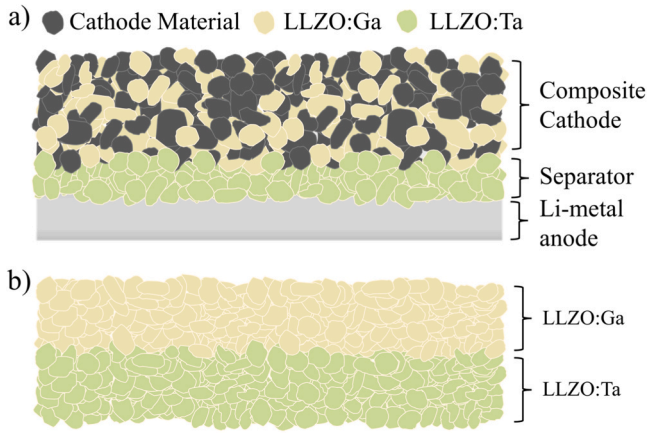

Fig. 1. Schematic cell setup with heterogeneous electrolytes. LLZO:Ga in the composite cathode and LLZO:Ta as separator with contact to the Li metal anode.

2.2. Characterization

To examine the cross-section microstructure, the samples were embedded in epoxy resin, cut and polished. Afterwards they were coated with a thin sputtered Au layer and analyzed with a scanning electron microscope (SEM) (EVO 15, Zeiss) with a backscattered electron detector, and energy-dispersive X-ray spectroscopy (EDX) was performed with an EDX detector (Ultim Max 100, Oxford Instruments). The electron acceleration voltage was always set to 15 kV. The density of the cathodes was analyzed with the ImageJ software. Raman spectroscopy mappings over the clean cross-sections were performed with the Raman device INVIA Qontor (Renishaw) with a wavelength of 532 nm and ~2.5 mW power and a 2400 l mm^{-1} grating. The spectra were collected with a step size of (x, y) = (1 µm, 1 µm) over the entire sample cross-section with a measuring time of 1 s per spectrum. The spectra were processed, including cosmic ray removal, and normalization. Electrochemical impedance spectroscopy (EIS) was performed with a VMP-300 (Biologic) in a climate chamber VT 4002EMC (Vötsch Industrietechnik) at 25 °C with a frequency varied from 3 MHz to 100 mHz and an electrical field perturbation of 10 mV. Polished cross sections of LLZO:Ta(0 %)|LLZO:Ga and LLZO:Ta(10 %)|LLZO:Ga embedded in epoxy resin were analyzed on a TOFSIMS.5 NCS system (IONTOF GmbH). Mass spectra were taken in positive polarity and the machine operated at a Bi^+ primary ion energy of 30 keV and an oxygen sputter energy of 2 keV. Charge compensation was accomplished by a low energy electron flood gun and Ar main flooding at a pressure of 1×10^{-6} mbar. The analyzed area was pre-sputtered to remove surface contaminations and subsequently analyzed in a 500 µm × 500 µm raster at a resolution of 1024 × 1024 pixels. A combination of spectrometry mode with reduced aperture was chosen to combine good lateral resolution and good mass resolution for large scale imaging.

3. Results and discussion

3.1. Microstructure

The optimal microstructure of co-sintered LLZO:Ga and LLZO:Ta is expected to be dense with a well-connected interface between LLZO:Ga|LLZO:Ta and a high phase purity of both components. To investigate the microstructure of the co-sintered samples, SEM images of the polished cross-section were made and compared with the pure sintered references of (LLZO:Ga, LLZO:Ta 0 %, and LLZO:Ta 10 %). The reference SEM images are shown in S-Fig. 1, and the density, porosity, and secondary

phase fraction values are given in Table 1. The sintered LLZO:Ga has a high porosity and also some secondary phases are located between the grains. Both LLZO:Ta materials show much higher densities >95 % without secondary phases, but a contrast difference is observable between grain interior and boundary region. This is already known from other reports [22,23,29], where a Ta enrichment in the grain interior results in the brighter contrast, while the reduced Ta concentration at the outer grain regions results in a darker contrast.

Cross-section SEM images of the co-sintered LLZO:Ga|LLZO:Ta samples are shown in Fig. 2a-d, with LLZO:Ta with brighter contrast on the left side (Ta-side) and LLZO:Ga with darker contrast on the right side (Ga-side). The microstructure of the two individual materials has changed drastically compared to the pure reference samples. The density of the individual LLZO:Ta sides is reduced to ~80 % (LLZO:Ta 0 %) and ~82 % (LLZO:Ta 10 %), while the density of the LLZO:Ga sides increased slightly. In addition, secondary phase formation, recognizable by a significantly different SEM contrast, increased to volume fractions of 0.3 % (LLZO:Ta 0 %) and 0.8 % (LLZO:Ta 10 %) for both samples. The fraction of secondary phases of the Ga-side co-sintered with LLZO:Ta 0 % decreased slightly to 0.1 %, while the fraction for the Ga-side co-sintered with LLZO:Ta 10 % increased to 0.8 %. The LLZO:Ga|LLZO:Ta interfaces are well-connected and sharp with no signs of secondary phases.

The deteriorated properties of the LLZO:Ta phase after co-sintering with the LLZO:Ga phase, such as the reduced sintering with the high relative porosity and the increased amount of secondary phases, have a detrimental effect on the cell performance as they reduce the ionic conductivity and decrease dendrite stability of the separators. The higher amount of secondary phases in the sample with 10 % Li excess is probably due to the changed chemistry of the LLZO:Ga system in Li-rich systems, where $LiGaO_2$ forms at the grain boundaries [19]. This phase could also hypothetically react further to form La- or Zr- containing phases, which could match the SEM contrast of the observed secondary phases.

3.1.1. Cation interdiffusion

The possible cation interdiffusion during co-sintering of the LLZO:Ga|LLZO:Ta samples was investigated using ToF-SIMS and EDX analysis. Fig. 3 shows the analysis of the LLZO:Ga|LLZO:Ta sample with 0 % Li excess on the Ta-side. The EDX analysis (Fig. 3b) and ToF-SIMS (Fig. 3d) show a homogenous distribution of Ga-ions on the Ta-side. In addition, Ta-ions have also moved to the Ga-side (Fig. 3c). However, the Ta distribution is more heterogeneous and only found at a few individual spots.

Similar results were found for the LLZO:Ga|LLZO:Ta sample with 10 % Li excess (Fig. 4). EDX and ToF-SIMS showed a homogenous distribution of Ga-ions on the Ta-side (Fig. 4b,d), and a punctual distribution of Ta within the LLZO:Ga (Fig. 4c). Comparing both samples (0 % and 10 %) the Ga distribution shows almost no difference, but the Ta distribution is lower in the samples with 10 % Li excess. The reasons for the different distribution of Ga- and Ta-ions in LLZO (the distribution of Ga-ions in LLZO:Ta is much broader than that of Ta-ions in LLZO:Ga) may be related to potential diffusion mechanism, behind the Ga-ion migration. In LLZO the Li^+ sites (at Wyckoff 24d and 96 h), are connected to each other and build a 3D-Li^+-ion channel in the lattice [9]. Ga^{3+}-ions are substituted at the Li^+ sites and can probably also diffuse through this 3D channels, which could explain the homogeneous distribution of Ga-ions in LLZO:Ta [9]. When Ga^{3+}-ions are moving to the LLZO:Ta side, some Li-ions may also diffuse to the LLZO:Ga side to compensate for charge neutrality. The presence of Ga-ions on the Ta:LLZO side may lead to the formation of $LiGaO_2$ and thus possibly reduce the stability of LLZO:Ta in contact with Li metal. In contrast to Ga^{3+}, Ta^{5+} substitutes the Zr^{4+} site (at Wyckoff 16b), where the Ta-ions are locked in [ZrO_6] octahedrons. Therefore, the Ta-ions are not homogeneously distributed in the LLZO:Ga layer. The punctual distribution of Ta inclusions within LLZO:Ga could be explained by undesired mixing during sample preparation.

Table 1
Density, porosity, and secondary phase fraction (identified by different contrast) from the image analysis with the ImageJ software.

Sample		Density	Porosity	Secondary Phases
LLZO:Ga		76.0 %	23.8 %	0.2 %
LLZO:Ta 0 %,		96.2 %	3.8 %	0 %
LLZO:Ta 10 %).		96.8 %	3.2 %	0 %
LLZO:Ga|LLZO:Ta 0 % Li-excess	Ga-side	80.8 %	19.1 %	0.1 %
	Ta-side	82.6 %	17.1 %	0.3 %
LLZO:Ga|LLZO:Ta 10 % Li-excess	Ga-side	82.3 %	17.1 %	0.6 %
	Ta-side	82.1 %	17.1 %	0.8 %

3.1.2. Phase composition

Since the Ga- and Ta-ions, which stabilize the cubic LLZO phase, diffuse away during co-sintering of differently substituted LLZO samples, it cannot be excluded that the cubic phase is partially transformed into a less ion-conductive tetragonal phase. Therefore, Raman spectroscopy mappings were performed over the cross-section area to obtain information about the phase composition of LLZO on both sides and the interface between the two phases after sintering.

The reference samples of Ta:LLZO and Ga:LLZO showed the typical signals of the high-temperature cubic, highly ion-conducting LLZO phase (space group *Ia*-3*d*) (Fig. 5a). The individual signals can be assigned to the following vibrational modes: La cations vibration at 106 cm^{-1} (T_{2g}) and 121 cm^{-1} (E_g); broad signals of O bending at 216 cm^{-1} (T_{2g}), and 250 cm^{-1} (A_{1g}) for LLZO:Ta, and 226 cm^{-1} (T_{2g}), and 252 cm^{-1} (A_{1g}) for LLZO:Ga; Li vibrational modes at 369 cm^{-1} (T_{2g}), 416 cm^{-1} and 511 cm^{-1} (E_g or T_{2g}) for LLZO:Ta, and 359 cm^{-1} (T_{2g}), 408 cm^{-1} and 512 cm^{-1} (E_g or T_{2g}) for LLZO:Ga; Zr-O bond stretching at 645 cm^{-1} (A_{1g}) for LLZO:Ta, and 639 cm^{-1} (A_{1g}) for LLZO:Ga; the TaO_6 octahedron stretching at 736 cm^{-1} is only present in the Ta-substituted LLZO [30–33]. The investigation of the individual Ta- and Ga-sides of the co-sintered samples revealed that the cubic LLZO phase was preserved, as shown in Fig. 5b.

Examination of the individual Ta:LLZO and Ga:LLZO sides of the co-sintered samples revealed that the cubic LLZO phase was preserved, as shown in Fig. 5b. However, if a tetragonal LLZO phase were to form due to the diffusion of Ga- or Ta-ion, it would most likely occur directly at the LLZO:Ga|LLZO:Ta interface. This region was therefore investigated in more detail. To identify the exact position of the interface in Raman mapping, the TaO_6 octahedron stretching at 736 cm^{-1}, which only occurs in the LLZO:Ta and therefore clearly shows the edge of this phase, was plotted as shown in Fig. 6a, and Fig. 6b. No tetragonal LLZO phase was found in the sample with 0 % Li excess. In the sample with 10 % Li excess, a small indication of the tetragonal LLZO phase was found directly at the interface, indicated by signal splitting of the La vibration signals [32] (Fig. 6c). However, this occurrence is only partial, which is why the concentration of the tetragonal phase at the interface is probably very low.

From the Raman spectroscopy analysis, it can be concluded that the stability of the cubic LLZO phase is maintained after co-sintering of the LLZO:Ga|LLZO:Ta samples and only the sample with 10 % Li excess in the LLZO:Ta phase shows a small indication of some tetragonal LLZO at the interface. It can be assumed that a higher concentration of Li ions at the interface leads to a diffusion of Ga ions from the LLZO bulk structure to the grain boundaries, resulting in a de-stabilization of the cubic LLZO structure and its transformation to the tetragonal phase [19]. No secondary phases were detected by Raman spectroscopy, although they are clearly visible in the SEM images (Fig. 2 and Fig. 3). It is possible that the Raman activity of the secondary phases is too low or that they overlap

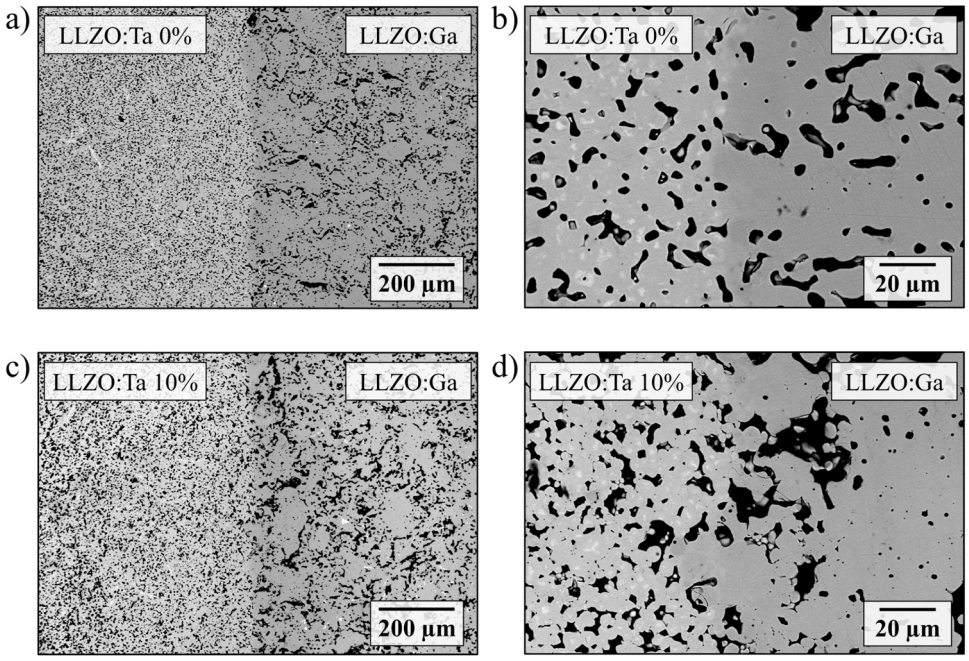

Fig. 2. Cross-section SEM images of the co-sintered samples with the 0 % Li excess in a) and b), and 10 % Li excess in c) and d). The LLZO:Ta side has the brighter contrast and the LLZO:Ga side has the darker contrast.

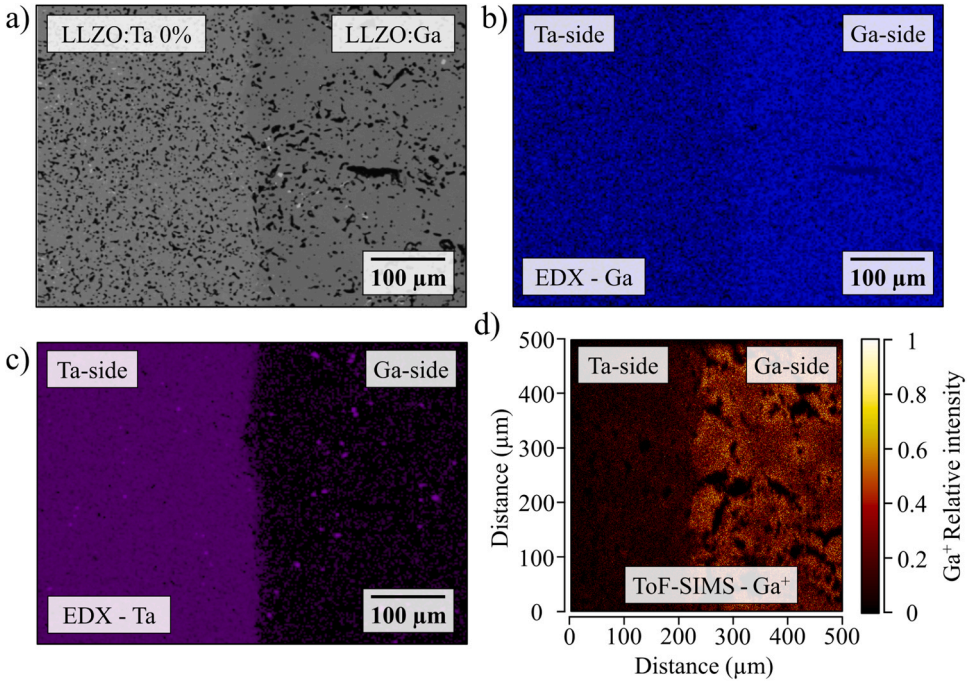

Fig. 3. Analysis of cation interdiffusion at the LLZO:Ga|LLZO:Ta interface of the sample with 0 % Li excess: a) SEM image of the EDX mapping area, b) EDX mapping of Ga, c) EDX mapping of Ta, d) ToF-SIMS mapping of Ga^+.

with the LLZO signals. For example, $LiGaO_2$ could be overlapped by the signals of Zr-O bond stretching [34].

3.1.3. *Ionic conductivity*

Since ionic conductivity is one of the most important properties of an electrolyte, EIS measurements were carried out on all reference samples and the co-sintered samples (Fig. 7).

The Nyquist plots of the EIS of all samples show only a semicircle and a Warburg-like impedance due to the gold coating of the pellets. The reference samples have a much lower resistance than the co-sintered samples, as can be seen in Fig. 7a. Fig. 7b with another scaling of the EIS data, shows the difference in resistance between the two co-sintered LLZO:Ga|LLZO:Ta samples. The first semicircle of the sample with 0 % Li excess shows a much larger ohmic resistance compared to the sample with 10 % Li excess. The corresponding total ionic conductivities of the different samples are shown in Table 2.

The drastically reduced ionic conductivity in the co-sintered LLZO:Ga|LLZO:Ta samples compared to the reference samples shows that the

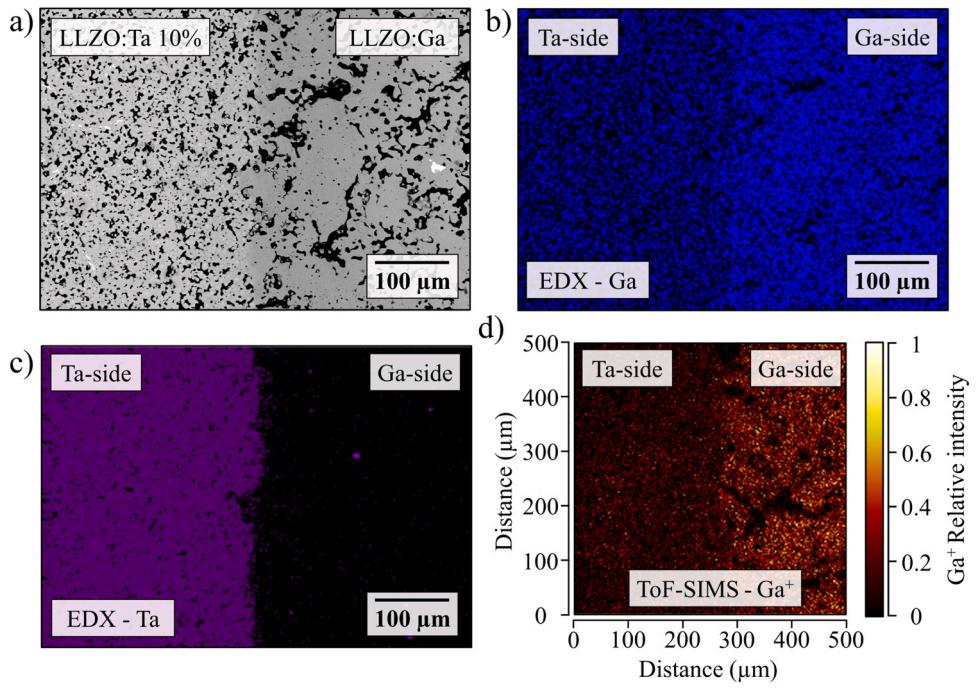

Fig. 4. Analysis of cation interdiffusion at the LLZO:Ga|LLZO:Ta interface of the sample with 0 % Li excess: a) SEM image of the EDX mapping area, b) EDX mapping of Ga, c) EDX mapping of Ta, d) ToF-SIMS mapping of Ga^{+}.

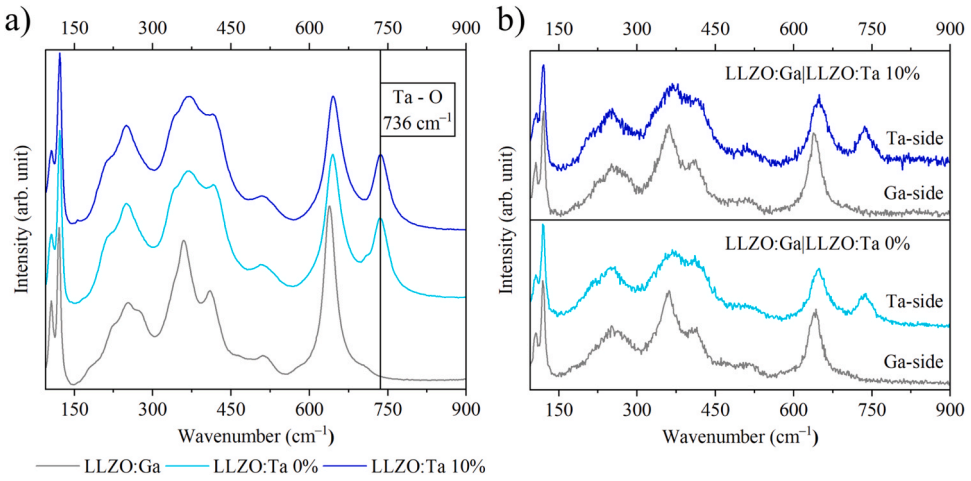

Fig. 5. Raman spectra of a) the pure reference samples, and b) both LLZO:Ga|LLZO:Ta samples with each respectively Ta- and Ga-side.

conventional co-sintering processing route does not appear to be suitable for processing heterogenous LLZO:Ga/LLZO:Ta electrolytes (Fig. 1a).

In an attempt to minimize the undesired ion cross-diffusion and phase transformation by lowering the sintering temperature, the pressure-assisted FAST/SPS sintering technique was used to sinter Ta:LLZO and Ga:LLZO powders. Surprisingly, this technique leads to much stronger interdiffusion, and unwanted reactions compared to the conventionally sintered powders. The LLZO:Ga side of the FAST/SPS sample appears black after sintering (S-Fig. 2) due to a large amount of secondary phases (S-Fig. 3a). In addition, the LLZO:Ga|LLZO:Ta interface was sintered less efficiently (S-Fig. 3b). The reason for the poorer sintering behavior is probably the reducing atmosphere during the FAST/SPS process carried out in Ar and in the presence of graphite foils. Therefore, other solutions are required to incorporate LLZO:Ga into functional LLZO-based cells. For example, the addition of SiO_2, which has been successfully used to sinter individual LLZO:Ga powders [19], can also be tested for sintering of LLZO powders with different substituents. Another potential solution could be the implementation of a protecting layer between the different LLZO compositions to prevent cation-diffusion. Such a protective layer could be for example MgO or Mg-substituted LLZO, since the Mg is also located at the Li^{+} sites it could potentially block Ga-ion movement. In addition, Ga^{3+} could react with MgO to form $MgGa_2O_4$ to anchor Ga-ions in the Mg protecting interface and preventing further diffusion to the anolyte.

4. Conclusion

The combination of different LLZO electrolytes for different functions in a cell is a very attractive concept that could improve the performance of ceramic batteries and enable the incorporation of LLZO:Ga as the garnet electrolyte with the highest ionic conductivity. Unfortunately, the results of this study show that the co-sintering of LLZO:Ga and LLZO:Ta powders leads to undesirable reactions, which are also

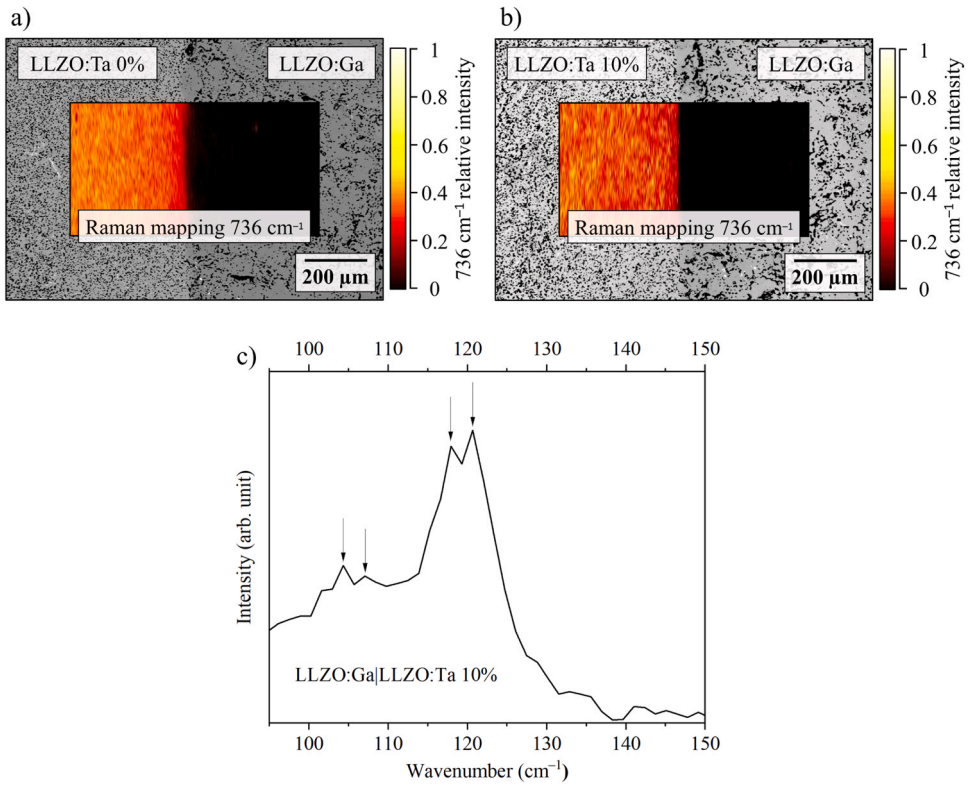

Fig. 6. Raman mapping with highlighted TaO_6 octahedron stretching at 736 cm^{-1} to find the LLZO:Ga|LLZO:Ta interface, overlayed in the corresponding SEM images: a) sample with 0 % Li excess, b) sample with 10 % Li excess, c) Raman spectra of the LLZO:Ga|LLZO:Ta 10 % Li excess interface with La vibration peak splitting.

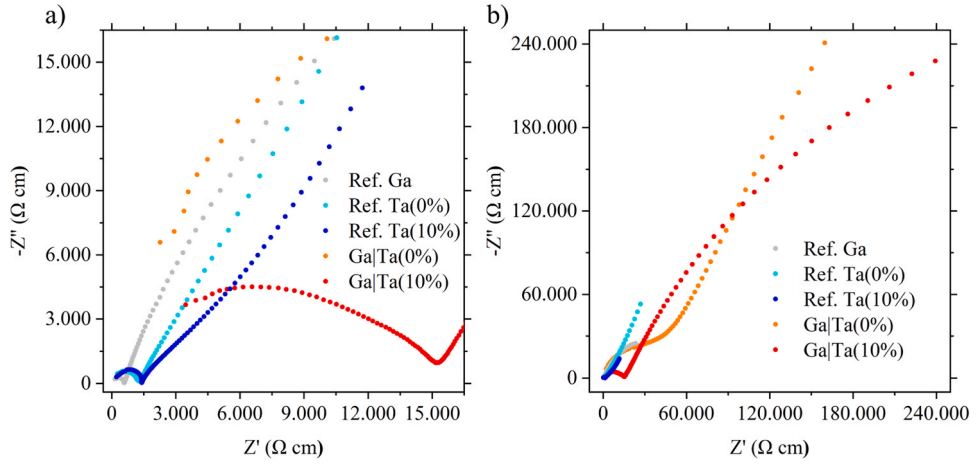

Fig. 7. Normalized Nyquist plot of the EIS measurements from the reference and co-sintered samples at 25 °C: a) region between 0 and 16.000 Ohm cm, b) larger resistance region shown (between 0 and 250.000 Ohm cm).

Table 2
Total ionic conductivity of the samples measured at 25 °C.

Sample	Total ionic conductivity (S cm^{-1})
LLZO:Ga	1.70×10^{-3}
LLZO:Ta 0 % Li excess	7.53×10^{-4}
LLZO:Ta 10 % Li excess	6.69×10^{-4}
LLZO:Ga|LLZO:Ta 0 % Li excess	1.60×10^{-5}
LLZO:Ga|LLZO:Ta 10 % Li excess	6.22×10^{-5}

influenced by the excess in Li concentration in the LLZO:Ta powder. The sintering activity of LLZO:Ta was reduced when co-sintered with LLZO:Ga powder, while the formation of secondary phase increased for both compositions. Strong interdiffusion of Ta- and Ga-ions was observed between differently substituted LLZO phases, which is expected to have a negative impact on the cell performance (e.g. reduced stability of LLZO:Ta towards Li metal due to the possible formation of a $LiGaO_2$). The cubic LLZO phase was mainly retained after sintering, but small signs of a tetragonal LLZO phase at the LLZ:Ga|LLZO:Ta interface were observed in the sample with 10 % Li excess. Finally, the ionic conductivity of the co-sintered samples was one order of magnitude lower than that of the reference LLZO:Ta and two orders of magnitude lower than

that of the LLZO:Ga reference. Our study showed that the conventional co-sintering of LLZO:Ga|LLZO:Ta components needs to be significantly improved before application.

CRediT authorship contribution statement

Sven Uhlenbruck: Writing – review & editing, Validation, Methodology, Conceptualization. **Martin Ihrig:** Writing – review & editing, Validation, Methodology, Investigation, Conceptualization. **Dina Fattakhova-Rohlfing:** Writing – review & editing, Validation, Funding acquisition. **Martin Finsterbusch:** Writing – review & editing, Methodology, Funding acquisition. **Christian Schwab:** Writing – review & editing, Visualization, Validation, Investigation. **Yannic Collette:** Writing – review & editing, Validation, Investigation. **Walter Sebastian Scheld:** Writing – review & editing, Writing – original draft, Visualization, Validation, Methodology, Investigation, Conceptualization.

Declaration of Competing Interest

The authors declare that they have no known competing financial interests or personal relationships that could have appeared to influence the work reported in this paper.

Acknowledgments

This work was funded by the German Federal Ministry of Education and Research (BMBF) as part of the FestBatt2-Oxide (grant no. 13XP0434A) and CatSE2 (grant no. 13XP0510A) projects, and by the Helmholtz Association of German Research Centers within the Helmholtz program “MTET: Materials and Technologies for the Energy Transition,” topic “Electrochemical energy storage”. The authors would like to thank Grit Häuschen for providing the LLZO:Ga powder.

Appendix A. Supporting information

Supplementary data associated with this article can be found in the online version at doi:10.1016/j.jeurceramsoc.2024.116936.

References

[1] J. Janek, W.G. Zeier, A solid future for battery development, Nat. Energy 1 (9) (2016).
[2] Y. Xiao, Y. Wang, S.-H. Bo, J.C. Kim, L.J. Miara, G. Ceder, Understanding interface stability in solid-state batteries, Nat. Rev. Mater. 5 (2) (2019) 105–126.
[3] N. Zhao, W. Khokhar, Z. Bi, C. Shi, X. Guo, L.-Z. Fan, C.-W. Nan, Solid garnet batteries, Joule 3 (5) (2019) 1190–1199.
[4] C. Wang, K. Fu, S.P. Kammampata, D.W. McOwen, A.J. Samson, L. Zhang, G. T. Hitz, A.M. Nolan, E.D. Wachsman, Y. Mo, V. Thangadurai, L. Hu, Garnet-type solid-state electrolytes: materials, interfaces, and batteries, Chem. Rev. 120 (10) (2020) 4257–4300.
[5] T. Thompson, S. Yu, L. Williams, R.D. Schmidt, R. Garcia-Mendez, J. Wolfenstine, J.L. Allen, E. Kioupakis, D.J. Siegel, J. Sakamoto, Electrochemical window of the Li-Ion solid electrolyte $Li_7La_3Zr_2O_{12}$, ACS Energy Lett. 2 (2) (2017) 462–468.
[6] R. Murugan, V. Thangadurai, W. Weppner, Fast lithium ion conduction in garnet-type $Li_7La_3Zr_2O_{12}$, Angew. Chem. Int. Ed. 46 (41) (2007) 7778–7781.
[7] M. Kotobuki, B. Yan, L. Lu, E. Hanc, J. Molenda, Study on stabilization of cubic $Li_7La_3Zr_2O_{12}$ by Ge substitution in various atmospheres, Funct. Mater. Lett. 9 (6) (2016) 1642005.
[8] L. Dhivya, K. Karthik, S. Ramakumar, R. Murugan, Facile synthesis of high lithium ion conductive cubic phase lithium garnets for electrochemical energy storage devices, RSC Adv. 5 (116) (2015) 96042–96051.
[9] L.J. Miara, W.D. Richards, Y.E. Wang, G. Ceder, First-principles studies on cation dopants and electrolyte|cathode interphases for lithium garnets, Chem. Mater. 27 (11) (2015) 4040–4047.
[10] C.-L. Tsai, Q. Ma, C. Dellen, S. Lobe, F. Vondahlen, A. Windmüller, D. Grüner, H. Zheng, S. Uhlenbruck, M. Finsterbusch, F. Tietz, D. Fattakhova-Rohlfing, H. P. Buchkremer, O. Guillon, A garnet structure-based all-solid-state Li battery without interface modification: resolving incompatibility issues on positive electrodes, Sustain. Energy Fuels 3 (1) (2019) 280–291.
[11] L. Dhivya, R. Murugan, Effect of simultaneous substitution of Y and Ta on the stabilization of cubic phase, microstructure, and $Li^{(+)}$ conductivity of $Li_7La_3Zr_2O_{12}$ lithium garnet, ACS Appl. Mater. Interfaces 6 (20) (2014) 17606–17615.
[12] M. Huang, M. Shoji, Y. Shen, C.-W. Nan, H. Munakata, K. Kanamura, Preparation and electrochemical properties of Zr-site substituted $Li_7La_3(Zr_{2-x}M_x)O_{12}$ (M = Ta, Nb) solid electrolytes, J. Power Sources 261 (2014) 206–211.
[13] S.F. Song, B.G. Yan, F. Zheng, H.M. Duong, L. Lu, Crystal structure, migration mechanism and electrochemical performance of Cr-stabilized garnet, Solid State Ion. 268 (2014) 135–139.
[14] C. Deviannapoorani, L. Dhivya, S. Ramakumar, R. Murugan, Lithium ion transport properties of high conductive tellurium substituted $Li_7La_3Zr_2O_{12}$ cubic lithium garnets, J. Power Sources 240 (2013) 18–25.
[15] K. Ishiguro, Y. Nakata, M. Matsui, I. Uechi, Y. Takeda, O. Yamamoto, N. Imanishi, J. Electrochem. Soc. 160 (2013) A1690–A1693.
[16] C.A. Geiger, E. Alekseev, B. Lazic, M. Fisch, T. Armbruster, R. Langner, M. Fechtelkord, N. Kim, T. Pettke, W. Weppner, Crystal chemistry and stability of "$Li_7La_3Zr_2O_{12}$" garnet: a fast lithium-ion conductor, Inorg. Chem. 50 (3) (2011) 1089–1097.
[17] M. Matsui, K. Takahashi, K. Sakamoto, A. Hirano, Y. Takeda, O. Yamamoto, N. Imanishi, Phase stability of a garnet-type lithium ion conductor $Li_7La_3Zr_2O_{12}$, Dalton Trans. 43 (3) (2014) 1019–1024.
[18] R. Wagner, G.J. Redhammer, D. Rettenwander, A. Senyshyn, W. Schmidt, M. Wilkening, G. Amthauer, Crystal structure of garnet-related Li-ion conductor $Li_{7-3x}Ga_xLa_3Zr_2O_{12}$: Fast Li-Ion conduction caused by a different cubic modification? Chem. Mater. 28 (6) (2016) 1861–1871.
[19] J. Li, H. Luo, K. Liu, J. Zhang, H. Zhai, X. Su, J. Wu, X. Tang, G. Tan, Excellent stability of ga-doped garnet electrolyte against Li metal anode via eliminating $LiGaO_2$ precipitates for advanced all-solid-state batteries, ACS Appl. Mater. Interfaces 15 (5) (2023) 7165–7174.
[20] C. Schwab, G. Häuschen, M. Mann, C. Roitzheim, O. Guillon, D. Fattakhova-Rohlfing, M. Finsterbusch, Towards economic processing of high performance garnets – case study on zero Li excess Ga-substituted LLZO, J. Mater. Chem. A 11 (11) (2023) 5670–5680.
[21] X. Tao, L. Yang, J. Liu, Z. Zang, P. Zeng, C. Zou, L. Yi, X. Chen, X. Liu, X. Wang, Preparation and performances of gallium-doped LLZO electrolyte with high ionic conductivity by rapid ultra-high-temperature sintering, J. Alloy. Compd. 937 (2023).
[22] W.S. Scheld, J.N. Ebert, M. Scherer, L. Fulanovic, L. Porz, C. Dellen, M. Ihrig, S. Uhlenbruck, M. Finsterbusch, O. Guillon, D. Fattakhova-Rohlfing, W. Rheinheimer, Blacklight sintering of garnet-based composite cathodes, J. Eur. Ceram. Soc. 44 (5) (2024) 3039–3048.
[23] W.S. Scheld, S. Lobe, C. Dellen, M. Ihrig, G. Hauschen, L.C. Hoff, M. Finsterbusch, S. Uhlenbruck, O. Guillon, D. Fattakhova-Rohlfing, Rapid thermal processing of garnet-based composite cathodes, J. Power Sources 545 (2022) 231872.
[24] M. Ihrig, M. Finsterbusch, C.-L. Tsai, A.M. Laptev, C.-h Tu, M. Bram, Y.J. Sohn, R. Ye, S. Sevinc, S.-k Lin, D. Fattakhova-Rohlfing, O. Guillon, Low temperature sintering of fully inorganic all-solid-state batteries – Impact of interfaces on full cell performance, J. Power Sources 482 (2021) 228905.
[25] C.-L. Tsai, E. Dashjav, E.-M. Hammer, M. Finsterbusch, F. Tietz, S. Uhlenbruck, H. P. Buchkremer, High conductivity of mixed phase Al-substituted $Li_7La_3Zr_2O_{12}$, J. Electroceram. 35 (1-4) (2015) 25–32.
[26] M. Mann, M. Kupers, G. Hauschen, M. Finsterbusch, D. Fattakhova-Rohlfing, O. Guillon, Evaluation of scalable synthesis methods for aluminum-substituted $Li_7La_3Zr_2O_{12}$ solid electrolytes, Materials 14 (22) (2021).
[27] M. Mann, M. Küpers, G. Häuschen, M. Finsterbusch, D. Fattakhova-Rohlfing, O. Guillon, The influence of hafnium impurities on the electrochemical performance of tantalum substituted $Li_7La_3Zr_2O_{12}$ solid electrolytes, Ionics 28 (1) (2021) 53–62.
[28] M. Ihrig, L.Y. Kuo, S. Lobe, A.M. Laptev, C.A. Lin, C.H. Tu, R. Ye, P. Kaghazchi, L. Cressa, S. Eswara, S.K. Lin, O. Guillon, D. Fattakhova-Rohlfing, M. Finsterbusch, Thermal recovery of the electrochemically degraded $LiCoO_2$/$Li_7La_3Zr_2O_{12}$:Al,Ta interface in an all-solid-state lithium battery, ACS Appl. Mater. Interfaces 15 (3) (2023) 4101–4112.
[29] W.S. Scheld, K. Kim, C. Schwab, A.C. Moy, S.K. Jiang, M. Mann, C. Dellen, Y. J. Sohn, S. Lobe, M. Ihrig, M.G. Danner, C.Y. Chang, S. Uhlenbruck, E. D. Wachsman, B.J. Hwang, J. Sakamoto, L.F. Wan, B.C. Wood, M. Finsterbusch, D. Fattakhova-Rohlfing, The Riddle of Dark LLZO: cobalt diffusion in garnet separators of solid-state lithium batteries, Adv. Funct. Mater. 33 (43) (2023) 2302939.
[30] G. Larraz, A. Orera, M.L. Sanjuán, Cubic phases of garnet-type $Li_7La_3Zr_2O_{12}$: the role of hydration, J. Mater. Chem. A 1 (37) (2013) 11419.
[31] S. Uhlenbruck, C. Dellen, S. Möller, S. Lobe, C.-L. Tsai, M. Finsterbusch, M. Bram, O. Guillon, Reactions of garnet-based solid-state lithium electrolytes with water — a depth-resolved study, Solid State Ion. 320 (2018) 259–265.
[32] T. Thompson, J. Wolfenstine, J.L. Allen, M. Johannes, A. Huq, I.N. David, J. Sakamoto, Tetragonal vs. cubic phase stability in Al – free Ta doped $Li_7La_3Zr_2O_{12}$ (LLZO), J. Mater. Chem. A 2 (33) (2014) 13431–13436.
[33] F. Tietz, T. Wegener, M.T. Gerhards, M. Giarola, G. Mariotto, Synthesis and Raman micro-spectroscopy investigation of $Li_7La_3Zr_2O_{12}$, Solid State Ion. 230 (2013) 77–82.
[34] L. Lei, H. Ohfuji, T. Irifune, J. Qin, X. Zhang, T. Shinmei, Disorder-activated Raman spectra of cubic rocksalt-type $Li_{(1-x)/2}Ga_{(1-x)/2}M_xO$ (M = Mg, Zn) alloys, J. Appl. Phys. 112 (4) (2012).